Proceedings of the 21st ICSMGE, Vienna, Austria, 14 – 19 June 2026. Pistrol, Adam & Schweiger (eds.)
Published by: ÖGG, Austrian Society for Geomechanics, Salzburg, Austria, ISBN 978-3-9503898-4-5
https://doi.org/10.53243/ICSMGE2026-1160

Insights into Landslide Reactivation: Monitoring and analysis of failure mechanisms using instrumentation

Asiri Karunawardena, Sanchitha Jayakody, Mihira Lakruwan
National Building Research Organisation, Colombo, Sri Lanka, asiri13@hotmail.com

Ryosuke Uzuoka
Disaster Prevention Research Institute, Kyoto University, Japan

ABSTRACT: A devastating rain-induced landslide occurred in Athwelthota, Sri Lanka, in May 2017, claiming multiple lives, causing severe infrastructure damage, and disrupting transportation in the area. In response, monitoring instruments were installed in 2022 on the adjacent slope under the Project RRLL, implemented within the SATREPS framework. This instrumentation setup, comprising surface inclinometers, borehole water level meters, tensiometers, and weather stations, was strategically deployed to assess the behavior of the slope identified as vulnerable to adverse weather conditions. While instruments are in place, the slope reactivated in June 2024 following prolonged rainfall, leading to further instability. Observations revealed that rainfall infiltration acted as an immediate trigger, but subsurface hydrology played a critical role in the slope failure. These findings corroborated the results of finite element analysis conducted for the 2017 landslide event, which highlighted the combined influence of hydrological and geotechnical factors on slope stability. Surface inclinometers installed 600 mm below the ground surface provided critical insights into the failure mechanism, showing progressive movements at failure initiation. Groundwater level readings further confirmed a rise in subsurface water levels, affirming the hydrological contribution to slope instability. These movements closely corresponded to periods of intense rainfall, underscoring the significant hydrological influence on the reactivation. The 2024 event offered a unique opportunity to validate the monitoring systems' performance. While they proved effective in identifying slope instability mechanisms, limitations in real-time data transmission hindered timely interventions and highlights the necessity of monitoring systems in locally identified unstable slopes.

KEYWORDS: Slope stability, Landslides, Instrumentation and Monitoring, Coupled Hydromechanical Analysis.

1 INTRODUCTION

Sri Lanka is a tropical island at the southern tip of the Indian peninsula. It usually receives year-round rainfall in different parts of the island. Among them, the southwestern monsoon, which activates from May to November, holds particular interest as it provides rainfall to landslide-prone areas. Even though every year records several landslide incidents during this period, the landslides that occurred in 2016 and 2017 were among the deadliest events in the last decade. In May 2017, there were eighteen (18) landslides in the Kalutara District of the Western Province, causing devastating losses. In particular, the Athwelthota Landslide was one of them, causing 9 fatalities, destroying 7 houses, and disrupting the road network in the area (Figure 1). According to meteorological data recorded at the automated rain gauge R43 (the closest rain gauge to the landslide), the rain spell started on 23rd May 2017. The cumulative rainfall after 70 hours was recorded as 380 mm, while on the 26th, rainfall intensified compared to antecedent conditions. These rain-induced rapid and long-travelling landslides (RRLL) became eye-opening events that highlighted the need to deal with landslides in a more proactive manner to minimize the enormous damage they cause.

The National Building Research Organisation (NBRO) collaborated with the International Consortium of Landslides (ICL) to study RRLLs in Sri Lanka and to provide an integrated solution to develop a landslide early warning mechanism under the SATREPs framework. This five-year research project started in March 2020 and was successfully completed in March 2025 (Konagai et al. 2023). Instrumentation and monitoring were major parts of this project to understand the causes of landslide initiation under local conditions. Under the RRLL project, the Athwelthota landslide was selected as one of the pilot sites to conduct further studies related to landslide initiation and flow dynamics. The instrumentation setup, comprising surface inclinometers, borehole water level meters, tensiometers, and weather stations, was strategically deployed to assess the behavior of the slope identified as vulnerable to adverse weather conditions (Dissanayaka et al. 2024). Unexpectedly, in June 2024, the Athwelthota landslide reactivated following a high-intensity rainfall event, with around 300 mm recorded on the 1st and 2nd of June (Figure 2). Interestingly, the surface inclinometer captured early movements of the landslide just before failure initiated.

These two events clearly demonstrate that rainfall infiltration has a direct impact on landslide initiation. However, what remains underexplored is the impact of hydrogeological conditions and how accurately local ground conditions need to be assessed to strategically place instrumentation. Therefore, this paper aims to study the role of hydrogeology in landslide initiation through numerical simulation and to analyze landslide reactivation using instrumentation data. This paper is structured as follows: Section 2 briefly describes the field investigation conducted and Section 3discusses reproducing initiation of the 2017 landslide, including geotechnical and hydrogeological assessments. Section 4 presents the instrumentation setup and Section 5 details its performance in detecting landslide reactivation.

Figure 1. Athwelthota Landslide happened in May 2017.

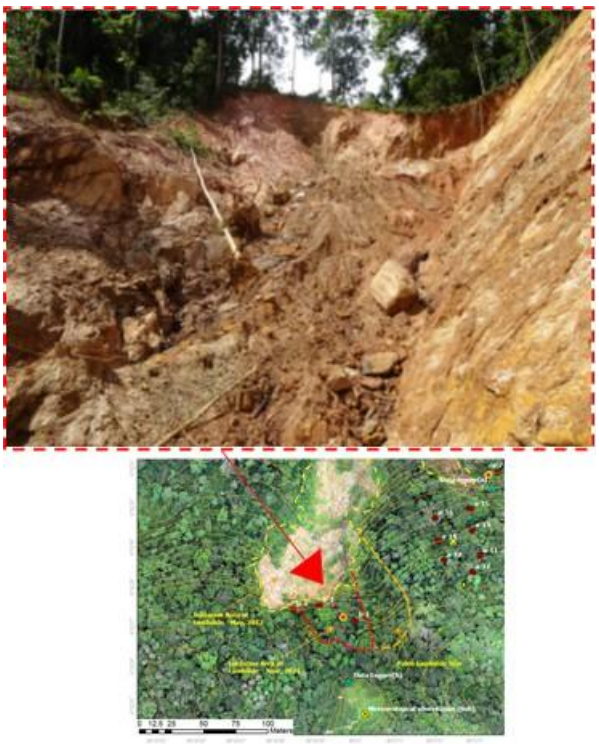

Figure 2. Athwelthota Landslide happened in June 2024

2 FIELD INVESTIGATION AFTER 2017 ATHWELTHOTA LANDSLIDE

2.1 *Geomorphology, geology, and soil profile of the area*

Figure 3 was prepared by overlaying a post-event drone image with a satellite image of the Athwelthota landslide area. The pre-event slope surface was obtained from the Survey Department of Sri Lanka, while the post-event profile was determined from a drone survey conducted by NBRO. The combined profiles indicated that the landslide extended approximately 176 m in length, with an average failed soil thickness of about 10 m. The pre-event slope angle was around 30°, as estimated from the available survey data.

The landslide occurred on an escarp slope within a region of dense vegetation, where the soils comprise sandy silt and clayey sand residual material mixed with weathered boulders. Field observations indicated that the underlying geology consists of moderately to highly weathered garnetiferous hornblende–biotite gneiss, with the weathering profile playing a key role in the landslide mechanism.

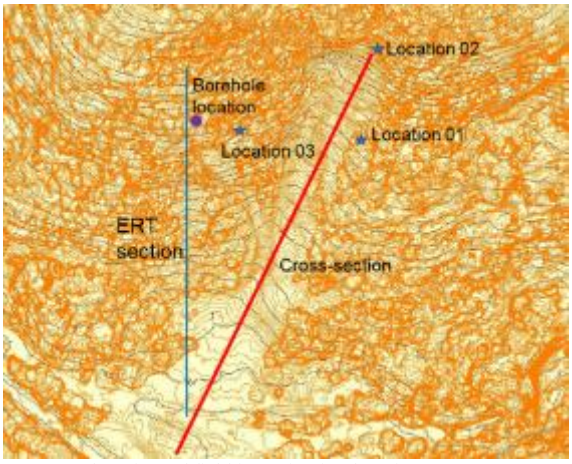

Figure 3. Plan view of field investigation locations

To further characterize the subsurface conditions, an electrical resistivity tomography (ERT) survey was conducted, revealing an irregular weathering profile: in some locations, bedrock is exposed at the surface, while in others it lies 10–12 m below ground level (Dissanayaka et al. 2024). Assuming similar geological layering in adjacent boundaries, a 24 m borehole was drilled to validate and compare the stratigraphy derived from the geophysical survey.

2.2 *Hydrological condition*

The landslide area is underlain by highly jointed, moderately to highly weathered bedrock that influences both groundwater behaviour and slope stability (Dissanayaka et al. 2024). The rock mass contains three main joint sets along with weak foliation planes, creating an interconnected network of fractures. These fractures provide pathways for water movement, affecting how groundwater flows through the slope and contributing to instability. The landslide catchment covers about 5 hectares, with a gentle slope, dense forest cover, and loose, organic-rich topsoil. Such conditions allow rainwater to infiltrate easily and recharge the underlying groundwater system. Compared to intact rock, the fractured bedrock has much higher permeability and porosity, enabling water to move and be stored more effectively. In this way, the jointed bedrock acts as a natural aquifer, retaining water near the unstable slope and releasing it gradually through springs into the valleys below. After the landslide, streams were observed emerging from fissures and fractures near the crown and discharging more heavily at the toe (Figure 4).

Figure 4. Springs emerge after the landslide

Groundwater monitoring conducted through borehole investigation revealed important characteristics of groundwater behavior under the weathered rock and bedrock regions, which are crucial for understanding hydrological behavior. As shown in Figure 5, groundwater is found at 7.60 m below the slope surface. However, water resistivity logging indicated specific depths within the hard rock strata where groundwater flows preferentially through fissures, termed the "fissured water" flow type. These observations validate the assumptions made during the numerical simulations in section 3, where nodes were adopted to apply groundwater flows that can emerge through the fissures and fractures.

2.3 *Residual soil characteristics*

The soils collected from the Athwelthota landslide were found to be Clayey Sand or Silty Sand. The soil has a specific gravity of 2.60 g/cm³ and a natural moisture content of 22%. The saturated hydraulic permeability, determined using the falling head method on remolded samples prepared to match the dry density of undisturbed specimens, averaged 3×10^{-5} m/s. For

numerical modelling, soil–water characteristic curve (SWCC) parameters based on the van Genuchten (VG) model were assumed from previous tests conducted on similar Sri Lankan soils. The SWCC was estimated using the modified Kovacs method proposed by Aubertin et al. (2003), which derives the function from the soil's saturated water content, particle size distribution, and liquid limit; the predicted curve was then calibrated to the VG model. Saturated consolidated undrained (CU) triaxial tests were performed under confining pressures of 50 kPa and 100 kPa to determine the shear strength parameters for use in slope stability analysis, using samples collected from Location 1 and Location 2 shown in Figure 3. Material parameters were calibrated through the element simulation method and results are presented in Figure 6 and Figure 7 (Jayakody et al. 2023).

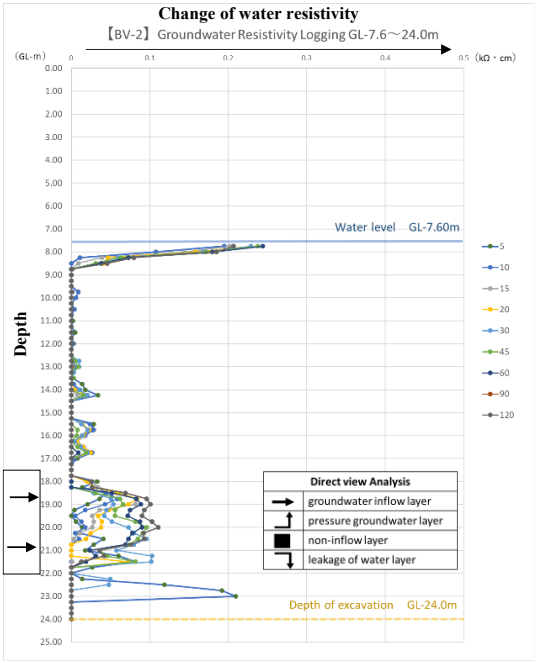

Figure 5. Groundwater monitoring in borehole

3 NUMERICAL SIMULATION OF 2017 ATHWELTHOTA LANDSLIDE

This section examines the effects of rainfall infiltration and the groundwater regime in relation to the Athwelthota landslide. The failure was influenced by numerous complex and partly unknown three-dimensional factors, including layered soil conditions, geological structures such as joints, fractures, and boulders, as well as site hydrology. For the purposes of analysis, however, the slope was simplified and modelled as a single homogeneous layer. Field observations suggested that the sliding surface developed along the soil–bedrock interface. The slope section used for the analysis was generated by comparing profiles from before and after the landslide, with the selected cross-section location shown in Figure 3. Although the landslide significantly altered the ground profile, the influence of bedrock geometry was not prioritized in this analysis.

Three-phase coupled hydromechanical finite element modeling (FEM), as outlined by Uzuoka and Borja (2012), was used to discuss the pre-failure behavior of the landslide subjected to the integrated effects of groundwater flow and rainfall infiltration (Jayakody et al. 2024). The Van Genuchten (VG) model (Genuchten, 1980), together with the unsaturated permeability function, was deployed to interpret the water retention behavior, and the extended modified Cam-Clay (MCC) model was utilized to simulate the mechanical behavior of the soil in the coupled FEM (Uzuoka et al. 2011). Material parameters used for the constitutive models are given in Table 1 and Table 2.

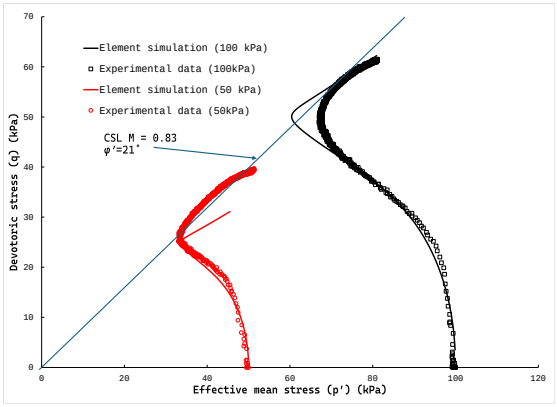

Figure 6. Stress path plots

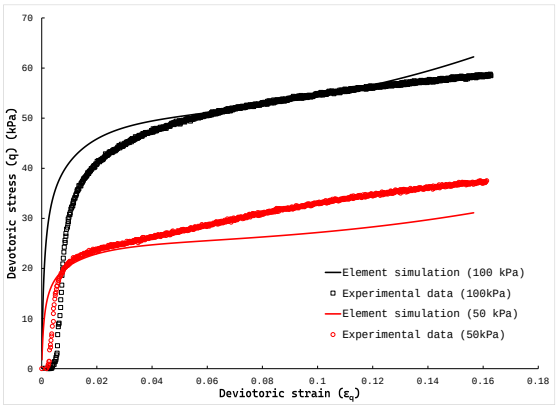

Figure 7. Stress-strain behavior

Table 1. VG model parameters

Parameter	Value
Minimum water saturation ($\boldsymbol{\theta_r}$)	0.25
Maximum water saturation ($\boldsymbol{\theta_s}$)	0.91
Parameters of VG model ($\boldsymbol{\alpha}$)	0.41
Parameters of VG model ($\boldsymbol{n}$)	2.2
Parameters of VG model ($\boldsymbol{m}$)	0.55

Table 2. Calibrated extended MCC parameters

Parameter		Value
Compression index, tangent of elastoplastic ln v – ln P, λ	calibrated	0.07
Swelling index, tangent of elastic ln v – ln P, κ	calibrated	0.021
Elastic shear modulus, μ_0	assumed	10 kPa
Elastic shear modulus parameter, μ_1	assumed	120
Reference elastic volumetric strain ε_{v0}^{e}		0
Reference mean effective stress, P_0		-1.0 kPa
Ratio of yield stress for mean effective stress at the start of calculation $\widetilde{P_{ct}}$/Pi	assumed	1.0
Critical state friction angle	calibrated	21°
Critical stress ratio, M = Q/P	calibrated	0.83
Isotropic evolution parameter of subloading surface, m_v	assumed	0.01
Parameter of unsaturated yield surface, a^c, b^c, p_{ref}	assumed	0.071, 1.6, 1.0

3.1 *Numerical model description*

The 2D plane strain model was generated from the geometry estimated by comparing the before and after topology of the area. Figure 8 presents the 2D plane strain FE model adopted in this analysis, which has dimensions equivalent to the actual slope failure. The bedrock is not included in the simulation. In the FEM isoparametric model, eight-node elements with an average span of 1 m on each side were used to create the computational mesh, consisting of 1,707 elements and 5,532 nodes.

As hydrological boundary conditions, nodes C, D, E, and F were assigned to apply total head to simulate groundwater flow. Rainfall was modelled as a flux boundary condition and was applied to the nodes H to I. Nodes from A to B were kept as the seepage boundary. Additionally, the soil–bedrock interface (B-C-D-E-F) was considered an impervious boundary condition. Air drainage was allowed only on the slope surface, and other boundaries were considered impermeable for the pore air boundary condition. As the displacement boundary condition of the soil skeleton, the nodes along the soil–bedrock interface (A-B-C-D-E-F) were fixed in both horizontal and vertical directions.

3.2 *Numerical Analysis*

During the numerical simulation, initial stress analysis was first conducted by gradually increasing the gravity from 0g to 9.81g. To minimize excessive plastic deformation incurred in this step, a saturated pre-consolidation stress of 50 kPa was applied. After the initial stress analysis, it was necessary to establish the initial condition, i.e., the distribution of water saturation in the slope, which is affected by rainfall infiltration and long-term groundwater flow conditions (Mori et al. 2011). Therefore, seepage analysis was conducted by applying the necessary boundary conditions for rainfall and groundwater flow. Because of the difficulty in reproducing actual rainfall in the recent past and the lack of records of groundwater flows, the rainfall and groundwater flows were assumed to be virtual. For the analysis, a rainfall of 7,500 mm per year over H-I region, which is typical in the area, and a total head of 94 m on node F were applied. After conducting the seepage analysis, hydromechanical analysis was carried out by applying recorded rainfall and total heads simultaneously. The total head values were determined by a trial-and-error method until the expected failure surface was generated and coincided with the time of failure.

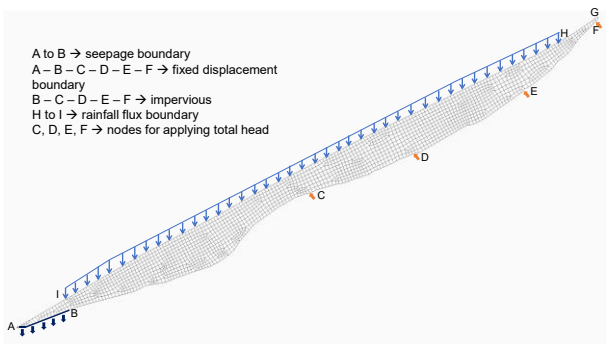

Figure 8. 2-D numerical model

3.3 *Numerical simulation results*

Figure 9 shows the deviatoric strain profile generated after 72 hours of rainfall. It depicts that the failure surface initiated from the soil–bedrock interface at the middle part of the soil slope. The progressive failure surface developed over time, starting from 68 hours, and at 72 hours the calculation was stopped due to non-convergence of the numerical simulation.

Figure 10 demonstrates the horizontal displacement of the slope at the time of failure. It shows that approximately 150 mm of displacement occurred in the middle part of the slope. This instability also caused some deformations in the top part of the slope, around 75 mm. A key observation during the analysis was that it was crucial to determine the total head values applied in order to reproduce both the failure surface and the seepage analysis results. Furthermore, it was understood that the failure at Athwelthota could not be reproduced solely by applying rainfall infiltration. Therefore, a proper understanding of local hydrological conditions is required to explain these complex phenomena.

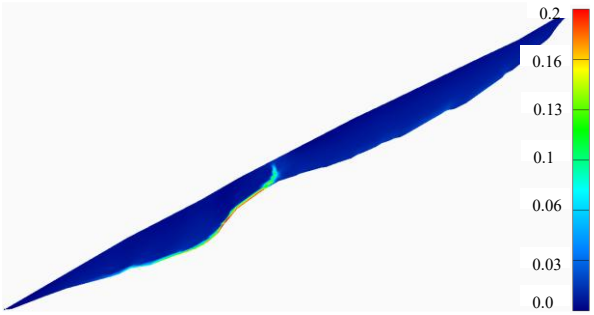

Figure 9. Deviatoric strain at the failure

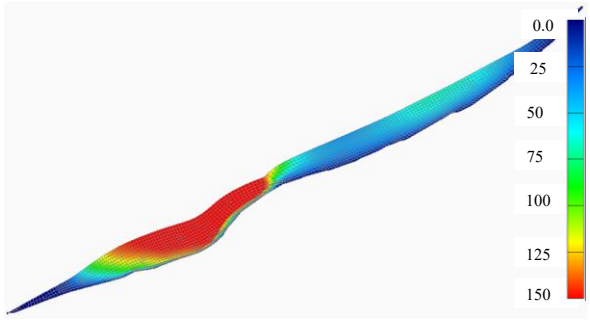

Figure 10. Horizontal displacement at the failure

4 INSTRUMENTATION SETUP

Understanding the hydromechanical processes that lead to landslides is critical for risk assessment and disaster mitigation in mountain and forested environments. This section focuses on monitoring rainfall-induced hydrological dynamics and surface as well as subsurface displacement on the slope adjacent to the Athwelthota landslide, which is susceptible to failure. The primary objective is to elucidate the relationship between rainfall characteristics, groundwater fluctuations, and slope movements to inform early warning and mitigation strategies. The monitoring network comprised borehole inclinometers and extensometers, surface extensometers, tensiometers, groundwater resistivity logging, and a meteorological station. Table 3 presents a summary of the instrumentation placed at the Athwelthota landslide site, as shown in Figure 11.

Table 3. Summary of instrumentation

Instrument	Installation details	Purpose
Tensiometers	Middle slope	Monitor soil moisture at multiple depths
Surface inclinometers	17 sensors on the middle slope, 3 sensors on scarp	Ground surface displacement
Borehole inclinometer & extensometer	Installed at 2 locations, depth up to 20 meters	Subsurface deformation and displacement monitoring

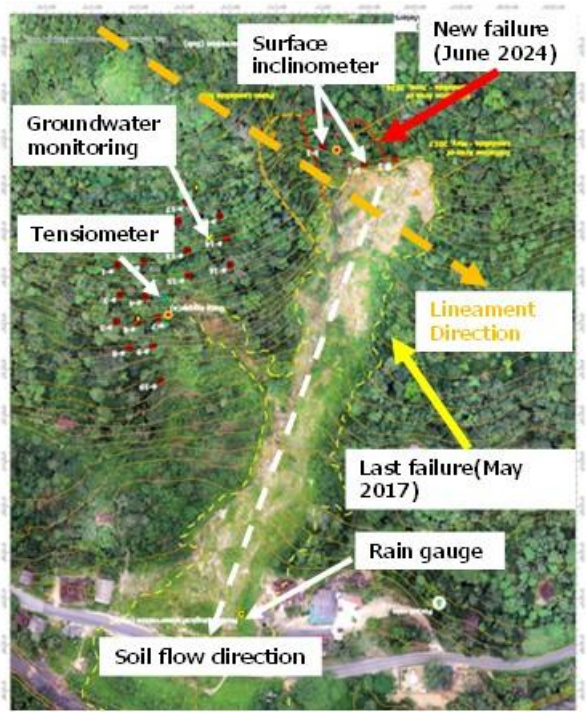

Figure 11. Instrumentation plan

5 MONITORING RESULTS AFTER 2024 ATHWELTHOTA LANDSLIDE

Figure 12 presents the fluctuations of subsurface hydrological response and slope movement with rainfall, monitored a few days before the landslide. Plot (a) shows the temporal distribution and intensity of rainfall events, while plot (b) illustrates the corresponding groundwater level fluctuations recorded in the borehole. Plot (c) presents matric suction changes at multiple depths within the slope, and plot (d) shows surface inclinometer inclinations. Together, these datasets allow a direct comparison of rainfall inputs with changes in groundwater table position and slope deformation, providing insight into the hydrological conditions leading to landslide initiation. Furthermore, it should be noted that only surface inclinometers were situated at the failure mass, while groundwater monitoring and tensiometers were located downslope.

5.1 *Groundwater fluctuations vs rainfall*

Groundwater levels stayed relatively stable until early May, despite intermittent rainfall. A distinct upward trend began in late May, closely following a sequence of high-intensity rainfall events shown in plot (a). The most rapid rise occurred after multiple consecutive rainy days, suggesting that infiltration overcame storage capacity in the unsaturated zone, causing a delayed but pronounced groundwater response. The peak groundwater level was reached shortly after the highest rainfall totals, indicating that percolation and recharge processes were active even after rainfall subsided. This rise not only indicates an increase in pore-water pressures but also reflects a bottom-up saturation process (Jayakody et al. 2024).

5.2 *Matric suction vs rainfall*

Matric suction decreased progressively at all monitored depths (0.5 m, 1.0 m, 2.0 m) during rainfall periods, with more pronounced drops observed during these times. The shallowest layer (0.5 m) responded most rapidly and strongly to rainfall, reflecting quick wetting and reduced negative pore pressure in the upper soil. Deeper sensors showed slower but steady decreases, indicating gradual infiltration. Notably, the lowest suction values coincided with the final sequence of intense rainfall, signaling near-saturation conditions. This demonstrates the development of a wetting front and increasing saturation as rainfall progressed.

5.3 *Surface inclination vs rainfall*

Surface inclinometer data show minimal changes throughout the monitoring period, despite a total accumulated inclination of around 1 degree. A marked acceleration in movement occurred in late May, aligning closely with both the peak rainfall events in plot (a) and the rapid groundwater rise in plot (b). The most significant displacement was recorded shortly after the heaviest rainfall, suggesting that slope movement was triggered by elevated pore pressures and reduced shear strength in the soil mass. The timing implies a short lag between hydrological loading and mechanical response, with displacement likely progressing as the slope structure adjusted to the reduced stability conditions.

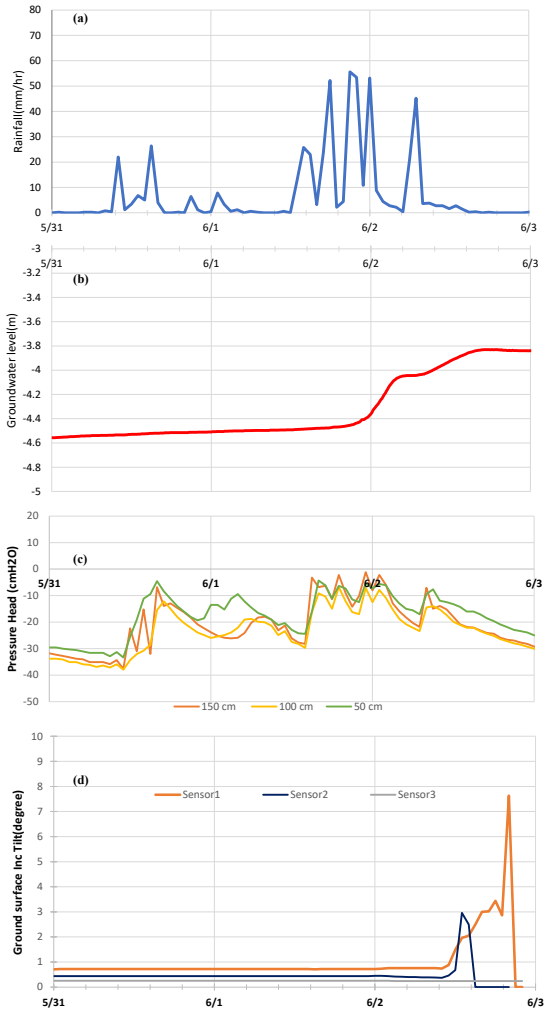

Figure 12. Rainfall, groundwater level, matric suction, and surface displacement onset of landslide. (a) Hourly rainfall intensity; (b) groundwater level variation in the borehole; (c) matric suction at 0.5 m, 1.0 m, and 2.0 m depths; (d) surface inclinometer displacement at monitoring points

6 CONCLUSION

This study of the Athwelthota landslide occurred in 2017 and 2024 demonstrates the critical role of coupled hydromechanical processes in slope failure. Field monitoring revealed that groundwater levels remained stable until late May 2024, after which a series of high-intensity rainfall events triggered a rapid rise, indicating a delayed but pronounced subsurface response and bottom-up saturation. Matric suction decreased progressively at all monitored depths, with the shallowest layer responding most rapidly, reflecting the development of a wetting front and increasing saturation. Surface inclinometer data indicated minimal initial displacement, but a marked acceleration occurred in late May 2024, coinciding with peak rainfall and groundwater rise, confirming that elevated pore pressures and reduced soil shear strength drove slope movement.

Numerical simulations conducted on failure happened in 2017 supported these observations, showing that the failure surface developed along the soil–bedrock interface and progressed under the combined effects of rainfall infiltration and groundwater flow. The analysis highlighted that reproducing the observed landslide behavior required both hydrological inputs and accurate representation of local groundwater conditions, indicating that rainfall alone was insufficient to trigger the failure.

Finally, the findings underscore the importance of integrating field monitoring with coupled hydromechanical modeling to understand landslide initiation, evaluate slope stability, and support early-warning and mitigation strategies. In complex terrains like Athwelthota, slope failure is governed not only by surface rainfall but also by subsurface hydrological conditions and soil–bedrock interactions, emphasizing the need for comprehensive site characterization for effective landslide risk management.

7 ACKNOWLEDGEMENTS

This research was supported by JSPS KAKENHI Grant Number 21H04575 and the Science and Technology Research Partnership for Sustainable Development (SATREPS), a collaboration between the Japan Science and Technology Agency (JST, JPMJSA1910) and the Japan International Cooperation Agency (JICA). The authors would like to acknowledge all project members of Project RRLL from the National Building Research Organisation and the International Consortium of Landslides for their support.

8 REFERENCES

Aubertin, M., Mbonimpa, M., Bussière, B., & Chapuis, R. P. (2003). Development of a model to predict the water retention curve using basic geotechnical properties. (Rapport technique n° EPM-RT-2003-01). https://publications.polymtl.ca/2604/.

Konagai, K. *et al.* (2023). Early Warning System Against Rainfall-Induced Landslide in Sri Lanka. In: Sassa, K., Konagai, K., Tiwari, B., Arbanas, Ž., Sassa, S. (eds) *Progress in Landslide Research and Technology, Volume 1 Issue 1*, 2022. Progress in Landslide Research and Technology. Springer, Cham. https://doi.org/10.1007/978-3-031-16898-7_16.

Dissanayaka, D.M.D.S., Weerasinghe, A.R.P., Jayakody, S.H.S., Asano, S., Bandara, K.N. (2024). Assessment of the Structural Geological, Hydrogeological, and Geomorphological Relationships of the Athwelthota Landslide, Sri Lanka. In: Abolmasov, B., *et al. Progress in Landslide Research and Technology*, *Volume 3 Issue 1*, 2024. Progress in Landslide Research and Technology. Springer, Cham. https://doi.org/10.1007/978-3-031-55120-8_21.

Jayakody, S., Uzuoka, R., Ueda, K. and Xu, J., 2023. Unsaturated slopes behavior under antecedent intermittent rainfall patterns: centrifuge and numerical study. *Acta Geotechnica*. doi:10.1007/s11440-023-02017-w.

Jayakody, S.H.S., Uzuoka, R. and Ueda, K., 2024. Effect of groundwater dynamics in rain-induced landslides: centrifuge and numerical study. *Soils and Foundations*, 64, p.101482. doi:10.1016/j.sandf.2024.101482.

Mori, T., Uzuoka, R., Chiba, T., Kamiya, K. and Kazama, M., 2011. Numerical prediction of seepage and seismic behavior of unsaturated fill slope. *Soils and Foundations*, 51(6), pp. 1075–1090. doi:10.3208/sandf.51.1075.

Uzuoka, R. and Borja, R.I., 2012. Dynamics of unsaturated poroelastic solids at finite strain. *International Journal for Numerical and Analytical Methods in Geomechanics*, 36(12), pp.1535–1573. doi:10.1002/nag.1061.

Uzuoka, R., Kazama, M. and Sento, N., 2011. Soil–water–air coupled analysis on seepage and overtopping behavior of river levee. In: *Proceedings of the 14th Asian Regional Conference on Soil Mechanics and Geotechnical Engineering (ARC 2011)*.

van Genuchten, M.T., 1980. A closed-form equation for predicting the hydraulic conductivity of unsaturated soils. *Soil Science Society of America Journal*, 44(5), pp.892–898. doi:10.2136/sssaj1980.03615995004400050002x.